Published in final edited form as:
Nature. 2009 January 8; 457(7226): . doi:10.1038/nature07520.

The dynein regulatory complex is required for ciliary motility and otolith biogenesis in the inner ear

Jessica R. Colantonio[1,*], **Julien Vermot**[4,*], **David Wu**[4], **Adam D. Langenbacher**[2], **Scott Fraser**[4], **Jau-Nian Chen**[2,3], and **Kent L. Hill**[1,3]

[1]Department of Microbiology, Immunology and Molecular Genetics, University of California, Los Angeles, California 90095, USA

[2]Department of Molecular, Cell, and Developmental Biology, University of California, Los Angeles, California 90095, USA

[3]Molecular Biology Institute, University of California, Los Angeles, California 90095, USA

[4]Biological Imaging Center, Beckman Institute, California Institute of Technology, Pasadena, California 91125, USA

Abstract

In teleosts, proper balance and hearing depend on mechanical sensors in the inner ear. These sensors include actin-based microvilli and microtubule-based cilia that extend from the surface of sensory hair cells and attach to biomineralized 'ear stones' (or otoliths)[1]. Otolith number, size and placement are under strict developmental control, but the mechanisms that ensure otolith assembly atop specific cells of the sensory epithelium are unclear. Here we demonstrate that cilia motility is required for normal otolith assembly and localization. Using *in vivo* video microscopy, we show that motile tether cilia at opposite poles of the otic vesicle create fluid vortices that attract otolith precursor particles, thereby biasing an otherwise random distribution to direct localized otolith seeding on tether cilia. Independent knockdown of subunits for the dynein regulatory complex and outer-arm dynein disrupt cilia motility, leading to defective otolith biogenesis. These results demonstrate a requirement for the dynein regulatory complex in vertebrates and show that cilia-driven flow is a key epigenetic factor in controlling otolith biomineralization.

Cilia are evolutionarily conserved organelles that perform motility, sensory and transport functions and are required for normal vertebrate development and physiology[2–5]. As such, cilium defects underlie a broad spectrum of human diseases[4,5]. Among the roles of ciliated organs in vertebrate embryogenesis, the contribution of cilia to inner-ear development remains poorly understood. In the zebrafish, *Danio rerio*, it has been proposed that beating cilia participate in the biogenesis of otoliths[6], which are analogous to otoconia in the otolithic membrane of human ears. These biomineralized particles provide an inertial mass that facilitates deflection of underlying microvilli and cilia, thereby initiating signalling

Correspondence and requests for materials should be addressed to: K.L.H. (kenthill@mednet.ucla.edu).
*These authors contributed equally to this work.2

Supplementary Information is linked to the online version of the paper at www.nature.com/nature.

Author Contributions J.R.C., J.V., D.W. and K.L.H. designed the experiments and interpreted the results. J.R.C, J.V. and D.W. conducted the experiments. J.V. and D.W. developed the equipment and systems for and performed *in vivo* video imaging for the quantitative flow study and analyzed the data with J.R.C., S.F. and K.L.H. A.D.L. assisted with *in situ* hybridization. A.D.L. and J.C. provided guidance on *gas8* morpholino injections. The manuscript was written by J.R.C., J.V., D.W. and K.L.H. All authors discussed the results and commented on the manuscript.

events that allow the brain to detect sound, gravity and linear acceleration[1,7–9]. During early development, nascent otoliths are formed from a pool of precursor particles and tethered to cilia in the otic vesicle[6]. So far, direct evidence for the necessity of ciliary motility in this process is lacking.

In protists, ciliary motility is controlled by the Dynein Regulatory Complex (DRC), which regulates axonemal dynein activity in response to signals from the radial spokes and central pair apparatus[10–15]. The DRC subunit trypanin is conserved across diverse phyla[15–18] and the vertebrate (human) trypanin homologue, growth arrest-specific 8 (here called GAS8, in line with the HUGO database, but also, and originally, designated GAS11) is a microtubule-binding protein localized to regions of dynein regulation in mammalian cells[19–21]. So far, however, a requirement for GAS8 and the DRC in vertebrates has not been established. We identified a single *trypanin* homologue in zebrafish encoding a protein that is 63.8% identical to the human GAS8 protein and 32.0% identical to trypanin from *Trypanosoma brucei* (Fig. 1). The sequence identity and conserved genomic structure (Fig. 2a)[15,22] indicate that this zebrafish protein, designated Gas8, is indeed a member of this conserved family of dynein regulatory proteins[13,15]. Maternal *gas8* transcripts are ubiquitous throughout the embryo during early development (Fig. 1b, c). By the 12-somite stage, however, expression becomes concentrated in the developing ears (Fig. 1d, arrow) and this persists through the 18-to 20-somite stage (Fig. 1e, Supplementary Fig. 1). Transcripts are also clearly present in the brain, neural tube and pronephric ducts (Fig. 1f–h). Therefore, *gas8* is expressed in ciliated tissues during zebrafish organogenesis.

To determine how loss of *gas8* expression affects zebrafish development we employed antisense morpholino oligonucleotides (Fig. 2). Hydrocephaly, neural tube cell death and left–right axis defects are common in ciliary morphants and mutants[3] and were evident in *gas8* morphants (Fig. 2, Supplementary Fig. 2). Given the high expression of *gas8* in the otic vesicle, we examined ear development more closely. By two days post-fertilization, inner-ear atrophy was evident *gas8* morphants. The length along the antero-posterior axis was 30% less than in control embryos (morphants, 52 ± 6 μm, $n = 15$; control, 73 ± 7 μm, $n = 8$; 24–27 hours post-fertilization (h.p.f.); see, for example, Figs 2e, f, 3a, b). By three days post-fertilization, exactly two otoliths were present in control zebrafish, one at the anterior end and one at the posterior end of the otic vesicle, positioned ventrally to a semicircular canal[6]. By contrast, *gas8* morphants had abnormal numbers of otoliths, fused otoliths, abnormally positioned otoliths and small otoliths (Fig. 2g–m). Examination of 24-h.p.f. and 27-h.p.f. embryos showed that the same spectrum of defects is evident during nascent otolith formation (Fig. 2n–p). The otolith phenotype is 95–100% penetrant and co-injection of *in-vitro*-transcribed *gas8* messenger RNA carrying five base-pair mismatch mutations to prevent morpholino hybridization rescued the defect in a majority of embryos (Fig. 2g). Because inner ear patterning is tightly linked with neuraxis patterning[23], we analysed markers for the hindbrain (*egr2b*), midbrain (*eng2a*), forebrain (*otx2*), inner-ear anterio-ventral area (*fgf8a*)[24] and inner-ear anterior/posterior extremity (*bmp4*)[25]. We did not detect differences between controls and *gas8* morphants (data not shown). Therefore, otolith defects are not due to abnormal neuraxis or inner-ear patterning.

We next asked whether otolith defects were due to improper formation or placement of cilia in the otic vesicle. By 24 h.p.f., two classes of cilia were visible in the otic vesicle[6] (Fig. 3a, Supplementary Movie 1). Numerous short cilia were dispersed throughout the otic vesicle, and small patches of longer, ‘tether’ cilia were found exclusively at the anterior and posterior poles. Between 19 and 27 h.p.f., small precursor particles coalesced on tether cilia to form anterior and posterior otoliths[6]. We examined cilia distribution and size in morphant embryos during the critical developmental window of 19–27 h.p.f., when cilia are postulated to function in otolith assembly. At the 20-somite stage (corresponding to ~19 h.p.f. in wild

type), control and morphant embryos had cilia in the developing otic vesicle (data not shown). *gas8* morphants were slightly developmentally delayed, a common feature of morphant fish. Hence, we staged embryos based on developmental progression defined in ref. 26. By 24 h.p.f., both short cilia and tether cilia were distinguishable at the correct locations in control and *gas8* morphant embryos (Fig. 3b, Supplementary Movie 2). Otic vesicle size was reduced as noted above, but we did not detect major length differences of cilia between control (tether, 5.9 ± 0.2 μm; short, 1.4 ± 0.1 μm; $n = 5$ embryos) and morphant (tether, 5.9 ± 0.4 μm; short, 1.2 ± 0.2 μm; $n = 7$ embryos) embryos. At later stages, tether cilia persisted whereas short cilia began to disappear as expected[6] in both control and morphant embryos (data not shown). Cilia were also observed in the pronephric ducts and neural tube in *gas8* morphants (data not shown). Therefore, loss of *gas8* expression did not prevent formation, maintenance or correct positioning of cilia.

Because protist GAS8 homologues, trypanin in *T. brucei* and paralyzed flagella 2 in *Chlamydomonas reinhardtii*, are specifically involved in controlling ciliary beat[13–15], we examined cilia motility directly using *in vivo*, high-speed video microscopy. In all control embryos, one to three beating tether cilia were detected near each nascent otolith (Fig. 3, Supplementary Fig. 3, Supplementary Movies 3–5). Beating cilia directly bore the forming otolith or were located nearby (5–10 μm distant), often causing the otolith itself to oscillate (Supplementary Movies 3, 5). These cilia beat with a frequency of 34 ± 6 Hz ($n = 20$) at 24 h.p.f. Short cilia were not motile (Supplementary Movie 6). This contrasts with a previous report suggesting that tether cilia are immotile whereas short cilia distributed throughout the ear are motile[6]. The reason for this discrepancy is not clear, but it is probably due to technical challenges associated with imaging cilia motility, which was inferred indirectly in the earlier work and imaged directly here. In *gas8* morphants at every stage examined (19–27 h.p.f.), a majority of embryos displayed immotile tether cilia (60%, $n = 30$; Fig. 3, Supplementary Fig. 3, Supplementary Movies 7–8). Commonly, *gas8* morphants displayed ectopic otoliths located at the base of non-motile tether cilia (Fig. 2o). In some cases, morphants harboured ectopic beating cilia (23%, $n = 30$). To confirm that the ear phenotype was due to cilia immotility and not loss of another, unknown *gas8* function, we knocked down two genes directly involved in cilia motility: the gene for leucine-rich repeat-containing 50 protein, *lrrc50*, an outer-arm dynein subunit shown previously to be required for cilia motility[27,28]; and the left–right dynein gene *dnah9*, a well-characterized motor protein involved in cilia motility[29]. The same results were obtained upon knockdown of *lrrc50* (Supplementary Figs 4, 5). Furthermore, simultaneous knockdown of *lrrc50* and *dnah9* had a synergistic effect, causing more significant motility and otolith defects than either single knockdown alone. These treatments neither affected brain development nor triggered neural tube cell death and pericardial oedema. In all cases, abnormal otolith size, number and positioning were directly correlated with defective ciliary motility in morphants (Supplementary Fig. 4).

Otoliths are composite crystals assembled from a common pool of small, precursor particles. We hypothesized that otolith defects in cilia morphants arise as a consequence of abnormal fluid flow and the concomitant failure to properly direct precursor particle movements. To test this hypothesis, we examined fluid flow patterns in the otic vesicle by tracking otolith precursors at high temporal resolution. A direct correlation between cilia beat and fluid flow was observed (Fig. 4, Supplementary Movies 9–11). In control embryos, the motion of precursor particles near the otolith was non-random, whereas those further away from the otolith exhibited Brownian motion (Fig. 4g, h, Supplementary Movies 9–10), consistent with a previous report[6]. Cilia beating triggers a local flow in the vicinity of the otolith, attracting precursors at the base of tether cilia and propelling them towards the otolith (Supplementary Fig. 6, Supplementary Movies 9–10). By contrast, in *gas8* morphants, particles near tether cilia exhibited purely diffusive behaviour (Fig. 4, Supplementary Movie 11). Therefore, the

absence of ciliary beating limits particles to random motion, leading to formation of ectopic aggregates.

Our results demonstrate that Gas8 is required for normal motility of cilia in the otic vesicle and that ciliary motility is essential for normal ear development. The otic vesicle is a closed epithelial organ and fluid flow within this vesicle has been suggested to contribute to otolith formation[6]. Our study provides direct experimental evidence in support of this hypothesis. On the basis of high-speed video microscopy of cilia motility and quantitative analysis of precursor particle movements in wild-type and *gas8* morphant embryos, we propose a new, cilium-dependent hydrodynamic mechanism for otolith biogenesis (Fig. 4). In this model, motility of tether cilia at the poles of the otic vesicle establishes a vortex that attracts otolith precursors (Fig. 4i, l), thereby biasing an otherwise random distribution of precursor particles and concentrating them near the two patches of tether cilia. This ensures preferential otolith seeding at the poles of the otic vesicle. At the otic vesicle poles, tether cilia motility further serves to disperse precursor particles locally and oscillation of the otolith increases effective contact area with precursors (Fig. 4j). Together, this prevents particles from sedimenting to form ectopic aggregates and promotes efficient uniform otolith growth. This model explains the different features of the otolith phenotype observed in *gas8* morphants (Fig. 4k, m).

Our findings add to a growing list of developmental processes requiring fluid dynamic inputs for proper growth and patterning, further showing that epigenetic cues are part of the embryonic developmental program. In humans, hearing and balance defects are common among the elderly and are the most frequent sensory hereditary defects in newborns[30]. Although human patients with ciliopathies have not generally been observed to have obvious hearing loss[4], our results should stimulate investigations to look for more subtle inner-ear changes. To conclude, our studies demonstrate a requirement for motile cilia in vertebrate ear development and suggest that DRC subunits should be considered as candidates for disease genes contributing to ciliopathies in humans.

METHODS

Zebrafish lines

Wild-type AB zebrafish were maintained and raised as described previously[31]. Dechorionated embryos were kept at 28.5 °C in E3 solution with or without 0.003% 1-phenyl-2-thiourea (PTU, Sigma) to suppress pigmentation. Embryos were staged according to somite number (S) or hours post-fertilization[31].

gas8 riboprobe generation and *in situ* hybridization

The predicted *gas8* gene transcript of zebrafish, *Danio rerio* (Ensembl Gene ID #ENSDARG0000004 0871), was obtained from the annotated Ensembl automatic analysis pipeline and predicted exon/intron boundaries, transcript size and predicted protein size were obtained as described previously[32]. *D. rerio gas8* complementary DNA in pME18S-FL3 (clone IMAGE:5410961) was subcloned into the expression vector pcGlobin2 by PCR amplification of *gas8* from pME18S-FL3 using SacII and XhoI flanked primers (5′ primer, CCCCGCGGGTGGAACAATTCAATGCATT; 3′ primer, CCGCTCGAGATTTGAAGAAGAAACAAACA). GAS8–pcGlobin2 was linearized using BamHI and the antisense digoxigenin-labelled full length riboprobe was transcribed using SP6 RNA polymerase (Promega). Whole-mount *in situ* hybridization was carried out essentially as described in ref. 33 using either the *gas8* probe or one of the following probes: *spaw, eng2a*, *otx2, egr2b, bmp4*, *fgf8a* (provided by L. Trinh). Embryos were fixed with 4% para-formaldehyde, digested with proteinase K, and hybridized with the probe at 67 °C.

Alkaline-phosphatase-conjugated anti-digoxigenin antibody (Roche) was used to detect the *gas8* signals. After staining with NBT/X-phosphate (Roche), embryos were refixed with 4% paraformaldehyde and stored in PBS buffer. For imaging, embryos were mounted in 3.5% methyl cellulose and photographed on a Zeiss Axioplan microscope equipped with a Zeiss AxioCam digital camera.

Morpholino antisense oligonucleotides

Morpholino antisense oligonucleotides were designed to either target the translation start site of the *gas8* mRNA (AUG MO) or to target the splice donor site of the second coding exon (SP MO) and were obtained from Gene Tools. *Gas8* AUG MO: GCGACGATTTTCTTTTTGGTGGCAT; *gas8* SP MO: CGTTACCGACAAAATACCTGCTCTT; *gas8* 5-bp mismatch AUG MO, used for rescue experiments: GCCACCATTTTGTTTTTGCTGGGAT; standard control MO: CCTCTTACCTCAGTTACAATTTATA. *lrrc50* SP MO: AATGTAGACACTAAAGTTACCTGCT; *lrrc50* 5-bp mismatch MO: AATcTAGACAgTAAAcTTAgCTcCT; *dnah9* AUG MO: CGGTTCCTGCTCCTCCATCGCGCCG. The morpholinos were diluted in 5 mM HEPES buffer, pH 7.6. Embryos were injected at the one- to four-cell stage with either 6 ng AUG MO, 4 or 5 ng SP MO, or 6 ng standard control MO or mismatch AUG MO. For morpholino amounts used in *lrrc50* and *dnah9* injections, see Supplementary Fig. 5. The first MO (SP MO) targets the splice junction between exons 2 and 3, causing abnormal RNA processing and yielding a predicted transcript with an early stop codon (Fig. 2a). The second MO (AUG MO) targets the translational start site (Fig. 2a). Splice interference by the SP MO was demonstrated by RT–PCR (Fig. 2b).

Microinjection of either MO consistently produced hydrocephaly, brain and neural tube cell death, pericardial oedema, curved body axis and otolith defects (Fig. 2 and data not shown). Left–right axis determination was also affected, as demonstrated by *in situ* hybridization with the *southpaw* protein, a nodal-related protein that is normally expressed in the left lateral plate mesoderm[34] (Supplementary Fig. 1).

RT–PCR

Primer pairs used in RT–PCR to investigate the knockdown efficiency of *gas8* SP MO are 5′-AATCGTCGCCGAAGGGCAAAAC-3′(forward in exon 2) and 5′-CTGCATTGTTGTGGCTGCAG-3′ (reverse in intron 2–3) or 5′-CTTGGTGGCGTTCCTCTACTTC-3′ (reverse in exon 3); these pairs yield no product (normal splicing) or 315 bp (abnormal splicing with intron 1 retained), and 258 bp (normal splicing) or 1,957 bp (abnormal splicing with intron 1 retained; too large to be amplified under conditions used), respectively. Primers used for *lrrc50* were (1) 5′-GATCGTATCCACATCGATGAACT-3′ (‘*lrrc50* – Forward’), (2) 5′-CTCCATTAGGCATTTTACATG-3′ (‘*lrrc50* – Intron 1’), and (3) 5′-CTGGGGCCTGAAGGCTTTATG-3′ (‘*lrrc50* – Exon 2’). Control primer pairs for amplification of *gapdh* transcripts were also used to amplify a 95-bp region: 5′-TGTGATGGGAGTCAACCAGGACAA-3′ (forward); 5′-TTAGCCAGAGGAGCCAAGCAGTTA-3′ (reverse).

Immunofluorescence

Embryos were fixed in 4% formaldehyde in PBS buffer for a minimum of 2 h, rinsed in methanol, permeabilized by proteinase K treatment, blocked in 10% goat serum in PBS buffer containing 1% DMSO and 0.1% Tween 20 for at least 1 h, and incubated with a 1:500 dilution of anti-acetylated alpha tubulin antibody (Sigma) overnight. Secondary antibody, anti-mouse IgG Alexa-Fluor 488 (Molecular Probes), was used at 1:200 dilution. Embryos

were then embedded in 1% low melting agarose and imaged on a Zeiss LSM 510 confocal microscope using a water immersion objective with numerical aperture 1.1 and magnification either ×40 or ×63. Confocal images were collected using Zeiss LSM 510 software. Images were processed using Imaris (Bitplane AG).

High-speed video microscopy

For video microscopy, fish were anaesthetized with 0.0175% tricaine and embedded in agarose wells using 0.7% low-melt agarose. As a test, imaging of embryos without anaesthetic did not affect cilia beating relative to anaesthetized animals. Particle tracking was performed using Imaris (Bitplane AG). Data were further analysed using Matlab scripts. One hallmark of purely diffusive systems is a non-zero mean displacement $\langle \Delta r(t) \rangle$ over extended periods of time. Thus, a marker for non-diffusive transport is a changing mean displacement over time. We measured $\langle \Delta r(t) \rangle$ over a range of elapsed times t. To determine with a single parameter whether the mean displacement changes over time, we calculated the average of this quantity, $\langle \langle \Delta r(t) \rangle \rangle$. If the particle is freely diffusing then $\langle \langle \Delta r(t) \rangle \rangle \approx 0$; if it is driven then $\langle \langle \Delta r(t) \rangle \rangle > 0$. Cilia motion displayed in Fig. 3g–j was obtained using the time-to-colour Matlab script (provided by M. Liebling). Time-to-colour visualizes moving objects by assigning a colour according to the point in the cycle from which the image was taken. The resulting coloured images are obtained by superimposing six frames of the image sequence plus a greyscale frame. The first frame is assigned blue and the last frame, which corresponds to the still frame, is assigned orange. Non-moving objects, therefore, look like noise whereas moving objects display coherent patterns.

Supplementary Material

Refer to Web version on PubMed Central for supplementary material.

Acknowledgments

We are grateful to R. Crosbie for discussions and encouragement throughout the course of the project. We thank I. Drummond and C. Nguyen for discussions and comments on the work. We are grateful to L. Trinh, O. Bricaud and A. Collazo for sharing reagents and for providing probes, as well as to all the members of the Fraser laboratory for discussions, in particular M. Liebling and W. Supatto for sharing Matlab scripts and comments. We are grateful to Z. P. Kabututu for performing the *lrrc50* reverse transcriptase PCR experiments. J.V. was supported by a fellowship from the Human Frontier Science Program, D.W. was supported by the NIH Medical Scientist Training Program at UCLA/Caltech. J.R.C. was supported by NIH RSDA training grant no. M07185 and a Warsaw Fellowship from the MIMG Department at UCLA. A.D.L is supported by an NSF fellowship. This work was supported by NIH grant R01 HL081799 (J.C.), NIH grant R01AI52348 and Beckman Young Investigator Award (K.L.H.).

References

1. Sollner, C.; Nicolson, T. Biomineralization: From Biology to Biotechnology and Medical Application. 2. Bauerlein, E., editor. Wiley-VCH; 2004. p. 229-242.
2. Satir P, Christensen ST. Overview of structure and function of mammalian cilia. Annu Rev Physiol. 2007; 69:377–400. [PubMed: 17009929]
3. Bisgrove BW, Yost HJ. The roles of cilia in developmental disorders and disease. Development. 2006; 133:4131–4143. [PubMed: 17021045]
4. Badano JL, Mitsuma N, Beales PL, Katsanis N. The ciliopathies: an emerging class of human genetic disorders. Annu Rev Genomics Hum Genet. 2006; 7:125–148. [PubMed: 16722803]
5. Fliegauf M, Benzing T, Omran H. When cilia go bad: cilia defects and ciliopathies. Nature Rev Mol Cell Biol. 2007; 8:880–893. [PubMed: 17955020]
6. Riley BB, Zhu C, Janetopoulos C, Aufderheide KJ. A critical period of ear development controlled by distinct populations of ciliated cells in the zebrafish. Dev Biol. 1997; 191:191–201. [PubMed: 9398434]

7. Haddon C, Lewis J. Early ear development in the embryo of the zebrafish, *Danio rerio*. J Comp Neurol. 1996; 365:113–128. [PubMed: 8821445]
8. Hughes I, Thalmann I, Thalmann R, Ornitz DM. Mixing model systems: using zebrafish and mouse inner ear mutants and other organ systems to unravel the mystery of otoconial development. Brain Res. 2006; 1091:58–74. [PubMed: 16529728]
9. Nicolson T. The genetics of hearing and balance in zebrafish. Annu Rev Genet. 2005; 39:9–22. [PubMed: 16285850]
10. Huang B, Ramanis Z, Luck DJ. Suppressor mutations in Chlamydomonas reveal a regulatory mechanism for Flagellar function. Cell. 1982; 28:115–124. [PubMed: 6461414]
11. Piperno G, Mead K, Shestak W. The inner dynein arms I2 interact with a “dynein regulatory complex” in Chlamydomonas flagella. J Cell Biol. 1992; 118:1455–1463. [PubMed: 1387875]
12. Gardner LC, O’Toole E, Perrone CA, Giddings T, Porter ME. Components of a “dynein regulatory complex” are located at the junction between the radial spokes and the dynein arms in Chlamydomonas flagella. J Cell Biol. 1994; 127:1311–1325. [PubMed: 7962092]
13. Ralston KS, Lerner AG, Diener DR, Hill KL. Flagellar motility contributes to cytokinesis in Trypanosoma brucei and is modulated by an evolutionarily conserved dynein regulatory system. Eukaryot Cell. 2006; 5:696–711. [PubMed: 16607017]
14. Hutchings NR, Donelson JE, Hill KL. Trypanin is a cytoskeletal linker protein and is required for cell motility in African trypanosomes. J Cell Biol. 2002; 156:867–877. [PubMed: 11864997]
15. Rupp G, Porter ME. A subunit of the dynein regulatory complex in Chlamydomonas is a homologue of a growth arrest-specific gene product. J Cell Biol. 2003; 162:47–57. [PubMed: 12847082]
16. Baron DM, Ralston KS, Kabututu ZP, Hill KL. Functional genomics in Trypanosoma brucei identifies evolutionarily conserved components of motile flagella. J Cell Sci. 2007; 120:478–491. [PubMed: 17227795]
17. Hill KL, Hutchings NR, Grandgenett PM, Donelson JE. T lymphocyte triggering factor of African trypanosomes is associated with the flagellar fraction of the cytoskeleton and represents a new family of proteins that are present in several divergent eukaryotes. J Biol Chem. 2000; 275:39369–39378. [PubMed: 10969087]
18. Ralston KS, Hill KL. Trypanin, a component of the flagellar dynein regulatory complex, is essential in bloodstream form African trypanosomes. PLoS Pathogens. 2006:2.10.1371/journal.ppat.0020101
19. Bekker JM, et al. Direct interaction of Gas11 with microtubules: Implications for the dynein regulatory complex. Cell Motil Cytoskeleton. 2007; 64:461–473. [PubMed: 17366626]
20. Colantonio JR, et al. Expanding the role of the dynein regulatory complex to non-axonemal functions: association of GAS11 with the golgi apparatus. Traffic. 2006; 7:538–548. [PubMed: 16643277]
21. Yeh SD, et al. Isolation and properties of Gas8, a growth arrest-specific gene regulated during male gametogenesis to produce a protein associated with the sperm motility apparatus. J Biol Chem. 2002; 277:6311–6317. [PubMed: 11751847]
22. Whitmore SA, et al. Characterization and screening for mutations of the growth arrest-specific 11 (GAS11) and C16orf3 genes at 16q24.3 in breast cancer. Genomics. 1998; 52:325–331. [PubMed: 9790751]
23. Bok J, Brunet LJ, Howard O, Burton Q, Wu DK. Role of hindbrain in inner ear morphogenesis: analysis of Noggin knockout mice. Dev Biol. 2007; 311:69–78. [PubMed: 17900554]
24. Leger S, Brand M. Fgf8 and Fgf3 are required for zebrafish ear placode induction, maintenance and inner ear patterning. Mech Dev. 2002; 119:91–108. [PubMed: 12385757]
25. Mowbray C, Hammerschmidt M, Whitfield TT. Expression of BMP signalling pathway members in the developing zebrafish inner ear and lateral line. Mech Dev. 2001; 108:179–184. [PubMed: 11578872]
26. Kimmel CB, Ballard WW, Kimmel SR, Ullman B, Schilling TF. Stages of embryonic development of the zebrafish. Dev Dyn. 1995; 203:253–310. [PubMed: 8589427]

27. Sullivan-Brown J, et al. Zebrafish mutations affecting cilia motility share similar cystic phenotypes and suggest a mechanism of cyst formation that differs from pkd2 morphants. Dev Biol. 2008; 314:261–275. [PubMed: 18178183]

28. van Rooijen E, et al. LRRC50, a conserved ciliary protein implicated in polycystic kidney disease. J Am Soc Nephrol. 2008; 19:1128–1138. [PubMed: 18385425]

29. Kawakami Y, Raya A, Raya RM, Rodriguez-Esteban C, Belmonte JC. Retinoic acid signalling links left–right asymmetric patterning and bilaterally symmetric somitogenesis in the zebrafish embryo. Nature. 2005; 435:165–171. [PubMed: 15889082]

30. Shastry BS. Mammalian cochlear genes and hereditary deafness. Microb Comp Genomics. 2000; 5:61–69. [PubMed: 11087173]

31. Westerfield, M. The Zebrafish Book: A Guide for the Laboratory Use of Zebrafish (Danio rerio). Univ. Oregon Press; 1993.

32. Curwen V, et al. The Ensembl automatic gene annotation system. Genome Res. 2004; 14:942–950. [PubMed: 15123590]

33. Chen JN, Fishman MC. Zebrafish tinman homolog demarcates the heart field and initiates myocardial differentiation. Development. 1996; 122:3809–3816. [PubMed: 9012502]

34. Drees BL, et al. A protein interaction map for cell polarity development. J Cell Biol. 2001; 154:549–576. [PubMed: 11489916]

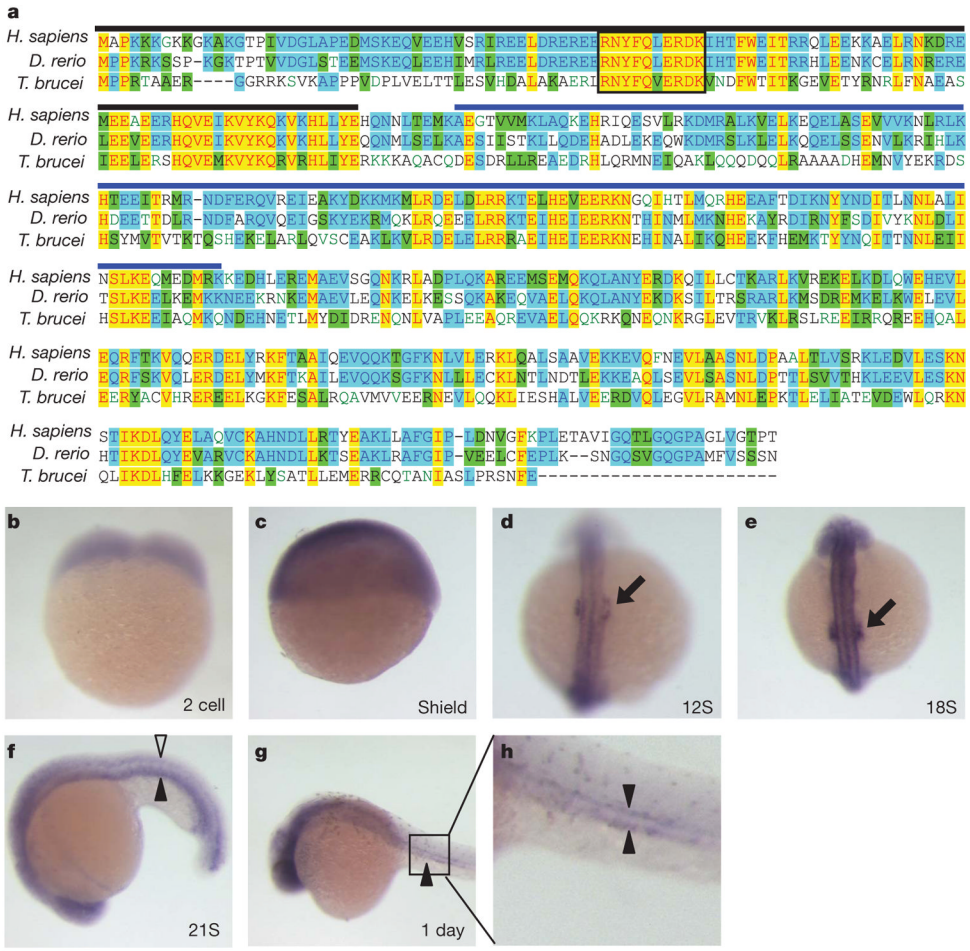

Figure 1. *gas8* is expressed in ciliated tissues

a, Protein sequence alignment of trypanin/GAS8 from *Homo sapiens*, *Danio rerio* and *Trypanosoma brucei*. Yellow highlighting indicates absolutely conserved residues, blue indicates residues conserved in two homologues and green indicates residues that are conservative substitutions. The boxed region indicates a conserved RNYFQERDK stretch that is found in every known trypanin/GAS8 homologue[17]. The conserved microtubule binding domain 'GMAD' and the regulatory domain 'IMAD'[19] are indicated with blue and black overlines, respectively. **b**–**h**, *In situ* hybridizations show the *gas8* expression pattern during the first 24 h of embryonic development. Developing ears (black arrows), neural tube (open arrowhead) and pronephric ducts (filled arrowheads) are shown. Developmental stages are indicated in each panel; S, somite. **h** is an enlargement of the boxed region in **g**.

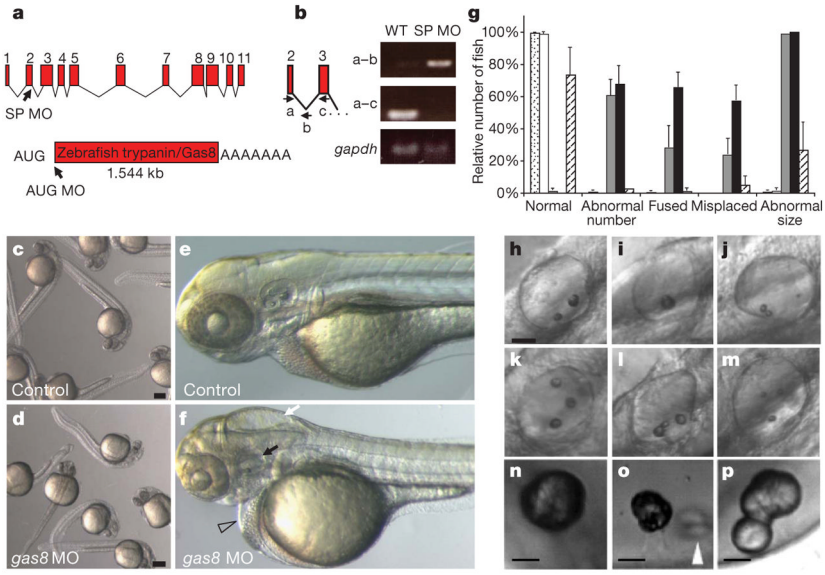

Figure 2. *gas8* morphants exhibit developmental defects

a, Intron/exon structure of the *gas8* locus, which encodes a predicted 1.54-kb transcript. The positions of splice blocking (SP MO) and translation blocking (AUG MO) morpholino oligonucleotides are shown. **b**, RNA from wild-type (WT) and *gas8* splice morphant embryos was analysed by PCR with reverse transcription (RT–PCR) using a forward primer (a) in the second exon and a reverse primer in either the second intron (b) or the third exon (c). In the morphant, blocking of the exon-2 splice donor site leads to a 315-bp RT–PCR product with the first primer set and no product with the second primer set. Controls for RT–PCR were provided by amplification of a 95-bp fragment of *gapdh*. **c**–**f**, *gas8* morphants have a variety of defects: overall morphology of controls (**c**) and *gas8* morphants (**d**) at 24 h.p.f.; detail of control (**e**) and morphant (**f**) embryos at 3 days post-fertilization (d.p.f.) showing hydrocephaly (white arrow), pericardial oedema (open arrowhead), disorganized somites and otolith abnormalities (black arrow). **g**, Quantitative analysis of otolith defects at 3 d.p.f. The relative number of fish having the indicated defect is shown for uninjected embryos (stippled bars; $n = 324$, five experiments), embryos injected with control MO (white bars; $n = 167$, two experiments), SP MO (grey bars; $n = 89$, two experiments), AUG MO (black bars; $n = 96$, two experiments) or co-injected with AUG MO and 250 pg *in-vitro*-transcribed *gas8* mRNA (hatched bars; $n = 225$, two experiments). Error bars, s.d. **h**–**p**, Panels show the spectrum of otolith defects observed in *gas8* morphants at 3 d.p.f. (**h**–**m**) and earlier times (**n**–**p**): normal otoliths (**h**); a single otolith (**i**); ectopic, fused and small otoliths (**j**–**m**); and nascent otoliths in control (**n**, 27 h.p.f.) and *gas8* morphant (**o**, 24 h.p.f.; **p**, 27 h.p.f.) embryos. Scale bars, 30 μm (**h**–**m**); 20 μm (**n**–**p**). White arrowhead indicates ectopic and fused otoliths in the *gas8* morphant. Embryos were injected with 6 ng (AUG MO), 4 or 5 ng (SP MO), 6 ng (standard control MO) or 6 ng (mismatch AUG MO) morpholinos.

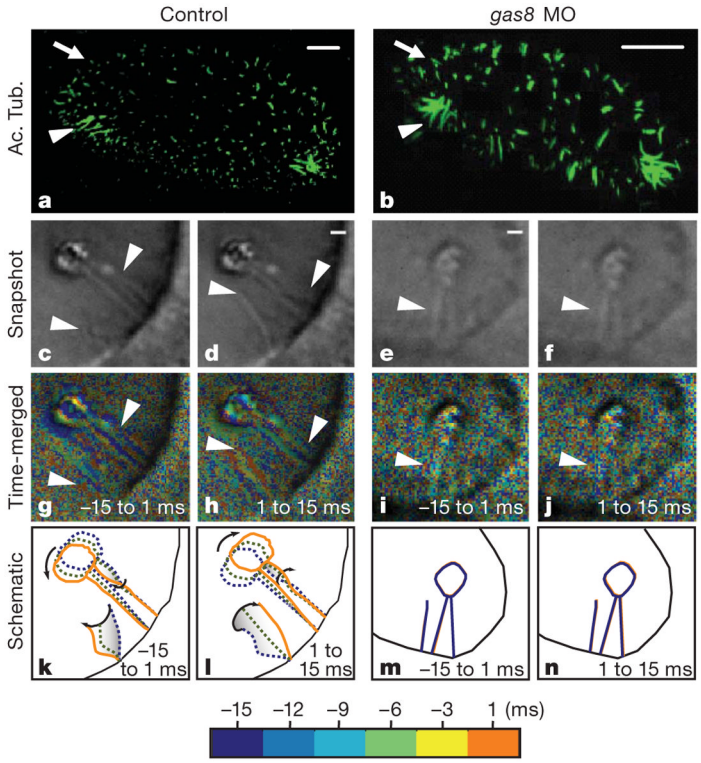

Figure 3. Gas8 is required for tether cilia motility

a, **b**, Cilia in control (**a**) and *gas8* morphant (**b**) embryos at 24 h.p.f., visualized by immunofluorescence labelling with anti-acetylated tubulin antibodies (Ac. Tub.). Arrowheads indicate the location of the tether cilia and arrows indicate short cilia. Scale bars, 10 μm. **c**–**n**, Tether cilia are motile in control embryos, but not in *gas8* morphants. Bright-field snapshot images from high-speed videos of cilia in controls (**c**, **d**) and *gas8* morphants (**e**, **f**), showing two steps of the cilia beat cycle with a 15-ms interval (half the period of a beat). **g**–**j**, Time-to-colour merge of six frames encompassing 15 ms of the cilia motion immediately preceding the still images shown in **c**–**f**, respectively. Cilia position in time is marked by different colours following the colour bar. When merged, moving objects are visible in the corresponding colours, whereas immotile objects only show background and noise. **k**–**n**, Diagrams showing cilia and otolith motion in control (**k**, **l**) and immotility in *gas8* morphant (**m**, **n**) embryos with three time points along half the period (15 ms) of the cilia beat cycle (see colour bar). Still images from control (**c**, **d**) and *gas8* morphant (**e**, **f**) embryos are taken from Supplementary Movies 3 and 5, respectively. Scale bars, 1 μm (**c**–**f**). Arrowheads point to tether cilia.

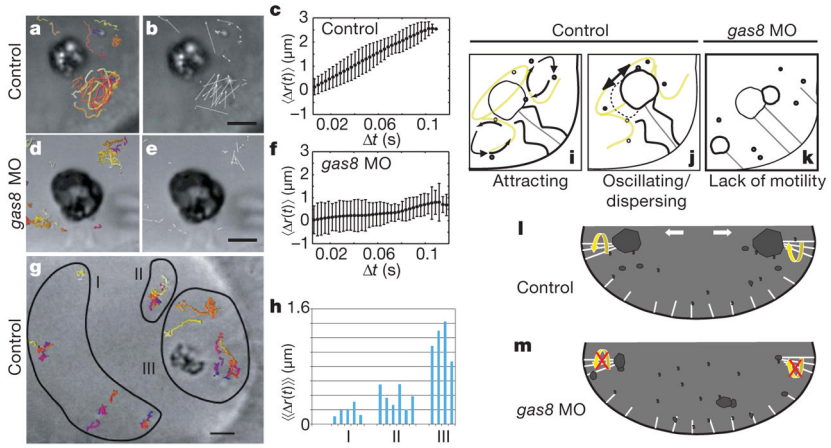

Figure 4. Tether cilia motility drives otolith biogenesis

a–**h**, Particle tracking analysis demonstrates that cilium-dependent fluid dynamics drive precursor particle movement near the otolith. In control embryos, particle tracks (**a**) and displacements (**b**) show that particles near the otolith move by non-Brownian motion. Each track has a different colour. **d**, **e**, In *gas8* morphants, particle tracks (**d**) and displacements (**e**) show decreased particle displacements in comparison with control. **c**, **f**, Mean particle displacement, $\langle \Delta r(t) \rangle$, plotted as a function of time. In control embryos, mean particle displacement is large and non-random, indicating diffusive transport. In *gas8* morphants, mean particle displacement is small and random, indicating Brownian motion only. Error bars indicate the variance in the calculation of $\langle \Delta r(t) \rangle$. **g**, **h**, Particle tracking in control embryos shows that particle displacement is directly correlated with position relative to the otolith. **g**, particle tracks. **h**, Displacements of particles in regions I, II and III of **g** were calculated as a function of time and the average of the mean displacement, $\langle \langle \Delta r(t) \rangle \rangle$, for each particle is shown. Net particle displacement decreases with increasing distance from tether cilia, indicating the reduction of the influence of ciliary beating. **i**–**k**, Diagrams depicting cilium-dependent otolith biogenesis. **i**, Tether cilia motility creates vortices that attract precursor particles. **j**, Cilia motility further serves to disperse particles locally and causes oscillation of the otolith, together facilitating uniform otolith growth. **k**, In *gas8* morphants, absence of ciliary motility limits particles to Brownian motion. **l**, In wild-type embryos, the net consequence of tether cilia motility is that precursor particles are concentrated near the tethers, preferentially seeding otoliths at two poles of the otic vesicle. **m**, In *gas8* morphants, loss of normal ciliary motility leads to formation of ectopic aggregates, non-uniform otolith growth and small particles that fail to coalesce into full-sized otoliths. Scale bars, 5 μm.